

Volume 3, Issue 5 — July — December-2016

**E  
C  
O  
R  
F  
A  
N**

**Journal-Bolivia**

ISSN-On line: 2410-4191

**ECORFAN®**



**ECORFAN®-Bolivia**

## **Indexing**

- Google Scholar
- Research Gate
- REBID
- Mendeley
- RENIECYT

## **ECORFAN-Bolivia**

### **Directorio**

#### **Principal**

RAMOS-ESCAMILLA, María. PhD

#### **CAO**

IGLESIAS-SUAREZ, Fernando. BsC

#### **Director of th Journal**

PERALTA-CASTRO, Enrique. MsC

#### **Logística Edition**

CLAUDIO-MENDEZ, Paul Armando. BsC

#### **Designer Edition**

LEYVA-CASTRO, Iván. BsC

**ECORFAN Journal-Bolivia**, Volume 2, Issue 3, July-December 2016, is a journal edited four- monthly by ECORFAN-Bolivia. Loa 1179, Cd. Sucre. Chuquisaca, Bolivia. WEB: [www.ecorfan.org](http://www.ecorfan.org), [revista@ecorfan.org](mailto:revista@ecorfan.org). Editora en Jefe: RAMOS-ESCAMILLA, María. PhD, Co-Editor: IGLESIAS-SUAREZ, Fernando. BsC. ISSN-On line: 2410-4191. Responsible for the latest update of this number ECORFAN Computer Unit. ESCAMILLA-BOUCHÁN, Imelda. PhD, LUNA SOTO-Vladimir. PhD. Loa 1179, Cd. Sucre. Chuquisaca, Bolivia., last updated December 31, 2016.

The opinions expressed by the authors do not necessarily reflect the views of the editor of the publication.

It is strictly forbidden to reproduce any part of the contents and images of the publication without permission of the National Institute of Copyright.

## **Editorial Board**

GALICIA-PALACIOS, Alexander. PhD  
*Instituto Politécnico Nacional, México*

NAVARRO-FRÓMETA, Enrique. PhD  
*Instituto Azerbaidzhan de Petróleo y Química Azizbekov, Russia*

BARDEY, David. PhD  
*University of Besançon, France*

IBARRA-ZAVALA, Darío. PhD  
*New School for Social Research, U.S.*

COBOS-CAMPOS, Amalia. PhD  
*Universidad de Salamanca, Spain*

ALVAREZ-ECHEVERRÍA, Francisco. PhD  
*University José Matías Delgado, El Salvador*

BELTRÁN-MORALES, Luis Felipe. PhD  
*Universidad de Concepción, Chile, Chile*

BELTRÁN-MIRANDA, Claudia. PhD  
*Universidad Industrial de Santander- Colombia, Colombia*

ROCHA-RANGEL, Enrique. PhD  
*Oak Ridge National Laboratory, U.S.*

RUIZ-AGUILAR, Graciela. PhD  
*University of Iowa, U.S.*

TUTOR-SÁNCHEZ, Joaquín. PhD  
*Universidad de la Habana, Cuba.*

VERDEGAY-GALDEANO, José. PhD  
*Universidad de Granada, Spain.*

SOLIS-SOTO, María. PhD  
*Universidad San Francisco Xavier de Chuquisaca, Bolivia*

GOMEZ-MONGE, Rodrigo. PhD  
*Universidad de Santiago de Compostela, Spain*

ORDÓÑEZ-GUTIÉRREZ, Sergio. PhD  
*Université Paris Diderot-Paris, France*

ARAUJO-BURGOS, Tania. PhD  
*Universita Degli Studi Di Napoli Federico II, Italy.*

SORIA-FREIRE, Vladimir. PhD  
*Universidad de Guayaquil, Ecuador*

FRANZONI-VELAZQUEZ, Ana. PhD  
*Instituto Tecnológico Autónomo de México, Mexico*

OROZCO-GUILLÉN, Eber. PhD  
*Instituto Nacional de Astrofísica Óptica y Electrónica, Mexico*

QUIROZ-MUÑOZ, Enriqueta. PhD  
*El Colegio de México, Mexico.*

SALAMANCA-COTS, María. PhD  
*Universidad Anáhuac, Mexico*

## **Arbitration Committee**

MTT, PhD

*Universidad de Granada, Spain*

AH, PhD

*Simon Fraser University, Canada*

AG, PhD

*Economic Research Institute - UNAM, Mexico.*

MKJC, MsC

*Universidad San Francisco Xavier de Chuquisaca, Bolivia*

MRCY, PhD

*Universidad de Guadalajara, Mexico*

MEC, PhD

*Universidad Anáhuac, Mexico*

AAB, PhD

*Universidad Autónoma de Sinaloa, Mexico*

EDC, MsC

*Instituto Tecnológico y de Estudios Superiores de Monterrey, Mexico*

JRB, PhD

*Universidad Panamericana, Mexico*

AGB, PhD

*Instituto de Biotecnología UNAM, Mexico*

ACR, PhD

*Universidad Nacional Autónoma de México, Mexico*

ETT, PhD

*CICATA-Instituto Politécnico Nacional, Mexico*

FVP, PhD. GHC, PhD. JTG, PhD. MMG, PhD

*Instituto Politécnico Nacional-Escuela Superior de Economía, Mexico*

FNU, PhD

*Universidad Autónoma Metropolitana, Mexico*

GLP, PhD

*Centro Universitario de Tijuana, Mexico*

GVO, PhD

*Universidad Michoacana de San Nicolás de Hidalgo, Mexico*

IAA, MsC

*Universidad de Guanajuato, Mexico*

IGG, MsC

*Centro Panamericano de Estudios Superiores, Mexico*

TCD, PhD

*Universidad Autónoma de Tlaxcala, Mexico*

JCCH, MsC

*Universidad Politécnica de Pénjamo, Mexico*

JPM, PhD

*Universidad de Guadalajara, Mexico*

JGR, PhD

*Universidad Popular Autónoma del Estado de Puebla, Mexico*

JML, PhD

*El Colegio de Tlaxcala, Mexico*

JSC, PhD

*Universidad Juárez del Estado de Durango, Mexico*

LCL Ureta, PhD

*Universidad de Guadalajara, Mexico*

MVT, PhD

*Instituto Politécnico Nacional, Mexico*

MLC, PhD

*Centro de Investigación Científica y de Educación Superior de Ensenada, Mexico*

MSN, PhD

*Escuela Normal de Sinaloa, Mexico*

MACR, PhD

*Universidad de Occidente, Mexico*

MAN, MsC

*Universidad Tecnológica del Suroeste de Guanajuato, Mexico*

MTC, PhD

*Instituto Politécnico Nacional -UPIICSA, Mexico*

MZL, MsC

*Universidad del Valle de México, Mexico*

MEC, PhD

*Universidad Autónoma de San Luis Potosí, Mexico*

NGD, PhD

*UDLA Puebla, Mexico*

NAL, MsC

*Universidad Politécnica del Centro, Mexico*

OSA, PhD

*Universidad Tecnológica Emiliano Zapata del Estado de Morelos, Mexico*

OGG, PhD

*Universidad Autónoma Metropolitana, Mexico.*

PVS, PhD

*Universidad Politécnica de Tecámac, Mexico.*

MJRH, PhD

*Universidad Veracruzana, Mexico.*

SCE, PhD

*Universidad Latina, Mexico.*

SMR, PhD

*Universidad Autónoma Metropolitana, Mexico*

VIR, PhD

*Instituto Mexicano del Transporte, Mexico*

WVA, PhD

*Universidad Politécnica Metropolitana de Hidalgo, Mexico*

YCD, PhD

*Centro Eleia, Mexico*

ZCN, MsC

*Universidad Politécnica de Altamira, Mexico*



## Presentation

ECORFAN Journal-Bolivia is a research journal that publishes articles in the areas of:

**E**ngineering **C**hemistry **O**ptical **R**esources **F**ood Technology **A**natomy and **N**utrition.

In Pro-Research, Teaching and Training of human resources committed to Science. The content of the articles and reviews that appear in each issue are those of the authors and does not necessarily the opinion of the editor in chief.

In Number 5 th presented in the first Section the article *Implementation of improvement in a production line for the production of meat in canal and primary cuts* by ANTONIO-ANTONIO, Alejandrina, MEZA –MORALES, Martha Isis, VAZQUEZ-FERNANDEZ, Jorge Alberto and RUIZ-PEREZ, Cinthia Daniela, in second Section the article *Orientation of nematic liquid crystals with spatially periodic anchoring* by CRUZ-DIOSDADO, Leonardo David, HERNANDEZ-LOPEZ, Eymard, MATIAS-GUTIERRES, Sergio and ROBERTO-LOPEZ, Castro, with adscription in the Tecnológico de Estudios Superiores del Oriente del Estado de México, in the third Section the article *Rehabilitation of manufacturing equipment* by CASTILLO-ORTIZ, Jorge Iram, ORTIZ-SIMÓN, José Luis and CRUZ-HERNÁNDEZ, Nicolás, with adscription in the Instituto Tecnológico de Nuevo Laredo, in the fourth Section the article *Structural characterization of CdS doped with Pb<sup>2+</sup>* by DÍAZ-REYES J', SÁNCHEZ-RAMÍREZ, J.F', FLORES-MENA, J.E" and MORÍN-CASTILLO, M.M", with adscription in the ' Instituto Politécnico Nacional and " Benemérita Universidad Autónoma de Puebla.

## Content

	<b>Article</b>	<b>Page</b>
Implementation of improvement in a production line for the production of meat in canal and primary cuts		1-6
Orientation of nematic liquid crystals with spatially periodic anchoring		7-15
Rehabilitation of manufacturing equipment		16-18
Structural characterization of CdS doped with Pb <sup>2+</sup>		19-28
<i>Instructions for Authors</i>		
<i>Originality Format</i>		
<i>Authorization Form</i>		

## **Implementation of improvement in a production line for the production of meat in canal and primary cuts**

ANTONIO-ANTONIO, Alejandrina, MEZA-MORALES, Martha Isis, VAZQUEZ-FERNANDEZ, Jorge Alberto and RUIZ-PEREZ, Cinthia Daniela

Received August 12, 2016; Accepted November 5, 2016

---

### **Abstract**

This research is the implementation of tools for process improvement in a company that is dedicated to the production, sale of meat carcasses, primal cuts, using flowcharts from the platform shipments, slaughter area, viscera , salted skins, boning area, performance area and conservation chamber and cooling in order to identify areas of opportunity for eliminate downtime, eliminate rework and identify opportunities for improvement using time and motion study for increase productivity within the company. The time and motion study was conducted throughout the process from the arrival of the beef until obtaining meat channel, all areas was analyzed to determine the time of each of the activities through random sampling for determine the standard time and distance of each activity today is of great importance to partake in continuous improvement to be more competitive in the workplace.

### **Enhancement tools, slaughter area, viscera, downtime and productivity**

---

**Citation:** ANTONIO-ANTONIO, Alejandrina, MEZA-MORALES, Martha Isis, VAZQUEZ-FERNANDEZ, Jorge, Alberto, RUIZ-PEREZ, Cinthia Daniela. Implementation of improvement in a production line for the production of meat in canal and primary cuts. ECORFAN Journal-Bolivia 2016, 3-5:1-6

---

---

\* Correspondence to Author (email: Alejandrina.antonio@upalt.edu.mx)

† Researcher contributing as first author.

## Introduction

The research was very useful because the results of implementing the improvement in a production line were obtained for the production of meat in the channel and primary cuts production process, from the entry of matter to finished product, using support tools such as diagrams of flow, at the same time was determined the standard time of each of the tasks of said process eliminated dead time, rework and waste. First, the study of each activity was done carefully and the time of each task was measured. The observation was carried out in a visual and random way. In this investigation, only the flow diagram of boning up to the stage of shipments is shown. It allows us to determine the activities of the process together with the help of the common chronometer. The chronometer is used to determine the standard time of each activity this allows us to optimize the process and increase the productivity of the same.

The objective of the improvement is to implement methods to optimize the production line to obtain the meat in the channel and the primary cuts from the entry of the raw material to finished product with the purpose of reducing downtime, eliminating rework and eliminating waste using Work tools such as flowcharts.

## Method description

Operator selection: workers must be able to perform their activities in the best possible way and above all must have good skill and effort. But nevertheless.

From any point of view, it is better that the method analyst should be based on the observations of an effective and cooperative worker working at the acceptable performance level, to achieve good results.

Show the working methods and readings of the time study: the time study should not be considered as a secret document confined to the use of analysts. It should be an accurate record of informative data covering the best and most efficient way of doing the work under the expected conditions when the work is being done.

Explanation to the operator and line supervisor: the analyst should be courteous, courteous and sincere to show recognition and respect for the problems of the operator, the analyst should be frank in dealing with the operator on matters of operations to be studied and on Time studies. The analyst must be able to explain in clear terms and without technicalities, all the actual timing procedures.

## Advantages of time study by element

- Evaluate performance more accurately.
- Determine changes in work items or their sequence when time standards have to be revised.
- Create standard time values for frequently recurring items; these can be checked against existing data, which helps to maintain the consistency of the data.
- Identify non-productive work.

**Timing record with the technique reset to zero**

This procedure is the one that gives the best result in general and in almost all elementary operations are recorded in the order in which they are performed and when taking time of an activity the timer should be left at zero to take the time of the other activities.

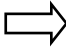





The method analyst lets the timer go through each activity throughout the study period, making the observation. You must do all this with enough speed and concentration to be free, in order to observe and write the time that the operation ends with the technique to zero. The zeroing technique does not provide the most accurate time of activities for each operation.

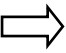



















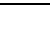
**Method Analyst Responsibilities**


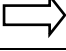
















1. Test, question and examine the current method, to ensure that it is correct in all respects before setting the standard.
2. Analyze with the supervisor, equipment, method and skill of the operator before studying operations.
3. Answer the questions related to the time study technique that could be made by the operator and the supervisor.
4. Always collaborate with the supervisor and the worker to get maximum help from them.
5. Abstracting from any discussion with the operator involved in the study or with the operators and what could be interpreted as criticism or censorship of the person.
6. Show the complete and accurate information in each study at the time made to specifically identify the method being studied.
7. Carefully note the measures of the times corresponding to the elements of the operation being studied.



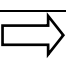
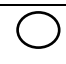

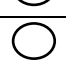


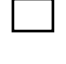


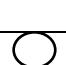
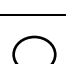

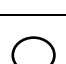


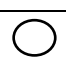
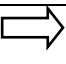
8. Evaluate with honesty and justice the activity of the operator.

Below is the flow diagram of the area of boning to the area of shipment anden, it is mentioned that the study was made in the whole process from the reception of the res to the boarding area and primary cuts. Only one part of the process is shown

Process Flowchart				
Diagram object: Area of Dehuee up to Anden de Embarques				
Part: First Method Diagram: Actual Sheet: 1 of 1				
The diagram begins in: conservation area				
The diagram ends in: shipping area				
Preparation: AAA date: _____		Preparation: AAA date: _____		
I hereby authorize: XXXX signature: _____				
#	Distance	Symbol	Time	Description
1	33.10 m		16.82 s	The area of conservation is transported the area of boning.
2	1.50 m		2.19 s	The piece of meat is sprayed into the canal to sanitize.
3			3.28 s	The channel is inspected for any dirt on the channel.
4	2.50 m		36.42 s	Cut the front quarter of the canal and cut the leg.
5			8.22 s	The leg is torn and deposited in the tare.
6			20.44 s	The front quarter of the channel is broken and is accommodated in the tare.

7	7.2m		17.71 s	It is transported in the mountains.
8	14 m		20.23 s	The beef leg is transported to the cutting area.
9	3.70 m		28.21 s	The front quarter is cut into 4 parts which is the chuck, neck, chest and crossbar.
10	14 m		1.29 s	It is deposited in the tare.
11	1.10 m		15.21 s	It takes time, because the operator is waiting for him to finish cutting the front room.
12			35.96	The front leg is boned.
13			1.10 s	The meat is sanitized
14			3.26 s	Cut some greasier parts.
15	2.10 m		11.53 s	Packaged
16			51.49 s	The bag is sealed
17			1.47 s	Fits in with the taras
18			31.37 s	The meat in the canal is transported to the area of desfalde
19			15.34 s	The skirt is cut
20			15.05 s	Delay, because the operator is waiting for other taras
21			15.91 s	Move the cutting area
22			28.27 s	Cut the greasier parts
23			2.19 s	Moves to the sanitization area
24			39.29 s	Packaged
25			51.49 s	The bag is sealed
26			15.77 s	Fits in with the taras
27	3.37 m		28.39 s	The other quarter of the channel is cut
28			16.94 s	The channel is cut

29			2.00 min	Delay, the operator leaves the work area
30			3.55 s	The channel is moved in the area of the saw.
31			7.28 s	Cut in the saw the 3 parts that are the rib, needle and thigh
32			3.47 s	Fits in with the taras
33	0.60 cm		37.15 s	The operator removes the tare and puts it on the work table to remove greasier parts
34			3.27 s	The sanitization area is moved
35	0.24 cm		25.36 s	It pockets
36			1.16 min	The bag is sealed
37			3.38 s	Inspected if well sealed
38			15.77 s	Fits in with the taras
39			5.27 s	Delay, the operator waits for the other operator to finish translating the tare
40			1.26 s	A small opening is made in the leg, to change the position of the roll
41	2.40 m		16.02 s	The ball that is next to the leg is cut
42	2.4m		28.00 s	The hip of the res
43	3.63 m		35.96 s	The leg of the beef is boned
44	0.70 cm		35.35 s	It is transported to the cutting area
45			5.28 s	Delay, because the operator performs another activity
46	3.63 m		7.27 s	The leg bone is removed and settled in the tare

47			36.24 s	It takes time, because you have to wait until the saw
48			9.47 s	The chamberete is started and deposited in the tare
49	7.30 m		11.24 s	It is transported in the mountains
50			6.24 s	The bone is cut (tuetano) and deposited in the tare
51	1.10 m		2.46 s	The chamberete cuts the greasier parts
52			3.26 s	The chamberete is sanitiza
53	2.80 m		5.24 s	The chamberete is pocketed
54	0.90 cm		51.49 s	The bag is sealed
55	0.30 cm		3.00 s	Sealing is inspected
56			15.77 s	Fits in with the taras
57			13.51 s	Moves to the waiting area
58			14.28 s	Tards are transported to the pre-cooling area
59			26.67 s	The boxes are assembled
60			68.78 s	The meat is accommodated in packaging boxes which is the chuck, half chest and needle
61			29.77 s	Fits the paw in the boxes and packs
62			68.78 s	Fits the front room, the shoulder, cross, neck and chamberete
63	35.20 m		3.11 min	Moves to the anden
64	0.60 m		24.22 s	Weighed and recorded
65	10 m		55.35 s	Is transported to the truck

**Table 1** Este diagrama muestra el proceso del área de deshuese hasta el andén de embarques

Summary			
Event	Number	Time	Distance
Operations	43	26.38 min	225.56 m.
Inspections	3		
Transport	13		
Delay	6		
Total	65		

**Table 2**

## Results

During the realization of this research of improvement in the production line, it was possible to determine the improvement of the production line with the determination of standard times of the different activities in the company from the entrance of raw material until obtaining meat in channel and cuts With a time of 52.7 min, salting of skins 2.59 min, area of boning 26.38 min, chamber of preservation 2.21 min, area of viscera 5.48 min, Yield 4.18 hours, this method is very important for the aforementioned areas because it facilitates the understanding of the workers and will know what activities to perform. It is also possible to have a control in the production areas and to correctly apply the procedure for the execution of tasks.

## Conclusions

This research used the flowchart to determine process optimization from the input of raw material to finished product, this facilitates the operarios to know what activity proceeds, also allows to detect process dead time, eliminate wastage and rework, and eliminate necks Of bottle

The tool was very useful for the development of the research of improvement in a production line for the obtaining of meats in channel and primary cuts, obtaining like result to determine the standard time of each area such as: 52.7 min of slaughter until Chambers pre-cooling / viscera, 2.59 min.

Salted from skin to shipments of skin, 28.59 min. In the area of boning until shipments of channels, 5.48 min. Chamber of viscera until shipments of viscera. 4.18 hours in the performance area. With a total of 5 hours, 49 min, 50 seconds.

Throughout the process, a sample of the diagram of a department is described, due to the confidentiality of the company. The good time analyst must have the mental capacity to analyze the most diverse situations and make the right and fast decisions. Have the necessary practical instruction in the area in which standards are to be established. For the company it was very useful to count the flow diagram because it allows them to know the process to be performed during the operation and facilitates the execution of tasks.

## **References**

Benjamín W. Niebel, A, 1990, Ingeniería Industrial, “Métodos, tiempos y movimientos” 9ª. Edición, edit. Alfaomega.

L.P. Alford. M.F. Dr.Eng. “manual de la producción” noriega editores.



## **Orientation of nematic liquid crystals with spatially periodic anchoring**

CRUZ DIOSDADO, Leonardo David †, HERNANDEZ-LOPEZ, Eymard, MATIAS GUTIERRES, Sergio and LOPEZ-CASTRO, Roberto

*Tecnológico de Estudios Superiores del Oriente del Estado de México*

Received June 3, 2016; Accepted November 26, 2016

---

### **Abstract**

Development of biosensors is one among many biomedical applications of liquid crystals. Recent simulation studies show that interactions at the interface between a nematic and a confining substrate (anchoring) enable us to detect sensitively the presence of biomolecules in complex samples. Yet, to the best of our knowledge, there is a scarcity of systematic studies of the effect of periodic modulation of surface anchoring for this kind of applications. Through simulations the final orientation fields can be predicted given certain initial conditions and detect the presence of disclinations in the liquid crystal. From the simulations carried out in this work, it is possible to predict the final orientation that the liquid crystal will present when it reaches the equilibrium as a function of the initial configuration which is very important for the development of biosensors

**Nematic liquid crystals, periodic anchoring, biosensors, biomolecules**

---

**Citation:** CRUZ DIOSDADO, Leonardo David, HERNANDEZ-LOPEZ, Eymard, MATIAS GUTIERRES, Sergio and LOPEZ-CASTRO Roberto. Orientation of nematic liquid crystals with spatially periodic anchoring. ECORFAN Journal-Bolivia 2016, 3-5:7-15

---

---

\* Correspondence to Author (email: diosdado1d@hotmail.com)

† Researcher contributing as first author.

## Introduction

In the field of liquid crystal based (CL) biosensors development, recent simulations and experiments have shown that the interactions at the interface between a nematic and the confining surface allow sensitively to detect the presence of biomolecules on the surface in very small concentrations.

By using numerical simulations and using coarse grain models, they suggest the possibility of controlling such sensitivity by spatially periodic anchoring patterns, however such simulations assume that the origin of such anchor is the periodic placement of binding sites for the biomolecules with a more precise beyond the current experimental techniques. As an alternative, it has been proposed to directly modify the chemical composition of the substrates to obtain anchor bands perpendicular and parallel to the substrate, alternately and periodically.

In addition to evaluating the effect of this type of anchoring conditions on the sensitivity of CL biosensors, periodic structures of the field of nematic orientation are of interest in the field of photonics. However, the nematic characteristically possess topological defects (disclinations) that can destroy the periodicity of the directing field.

To explore and understand the behavior of systems under such anchoring conditions at the CL interface with the confining surface, it is proposed to study the effect on the structure of the orientation field of the liquid crystal in models for CL biosensors.

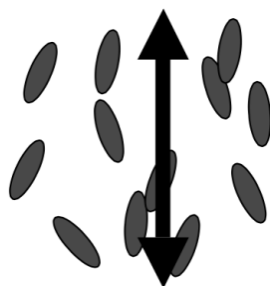
Specifically, this work simulates the temporal evolution of the liquid crystal system from controlled initial conditions, observing the effect on the final orientation structure of the LC associated with three classes of initial configuration: homeotropic, planar and random. The temporal evolution numerically solved the Beris-Edwards equations for a nematic by the finite difference method.

The methods and programs developed in this project can be applied later to problems of photonics, if they are combined with methods to calculate the structure of bands corresponding to different wavelengths of incident light in this type of devices.

## Cementitious Fluid Crystals

The main characteristic of Nematic Liquid Crystals (NLC) is that its molecules are highly anisotropic, usually they can be elongated in bar form, flattened in the form of disc or other more complex as banana form, besides being highly sensitive To electric and magnetic fields.

Another important aspect of NLC is that its molecules have no positional order, but they do tend to be oriented in the same direction (uniaxial), that is, the mass centers of the molecules are placed as in a liquid (without order) and the axes Principal molecules point, on average, along a particular direction called director  $n$  as seen in Figure 1.



**Figure 1** Vector director  $\mathbf{n}$ .

One way of describing how ordered the molecules are is by the order parameter  $S$ .

$$S = \frac{1}{2} \langle 3 \cos^2 \theta - 1 \rangle \quad (1)$$

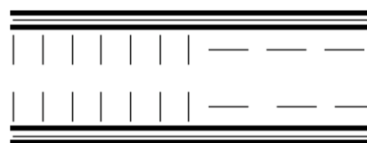
$$= \int \frac{1}{2} (3 \cos^2 \theta - 1) f(\theta) d\Omega$$

Where  $\theta$  is the angle of the principal axis of each molecule with respect to the director and the average is performed on the orientation  $\Omega$  of all molecules of the system. The value  $S = 1$  represents a total order of the molecules while  $S = 0$  means that the molecules are totally disordered.

### Periodic Space Anchors

With regard to anchoring, this refers to how the director is oriented on the surface that confines the liquid crystal. Thus, when referring to spatially periodic anchoring we mean that there will be alternating regions on the surface that confines to the NLC where the anchoring is of one or the other type.

Basically in this project we will focus on two types of alignment of the director on the surfaces that confine the LC: homeotropic anchorage, where the alignment is perpendicular to the surface, and homogeneous anchorage where the alignment is parallel to the surface (also called planar anchorage). Figure 2 shows a system confined to two surfaces (one at the top and one at the bottom). Each surface has two types of anchor: on the left side the anchorage is homeotropic and the right side is homogeneous. Applying periodic boundary conditions in the horizontal direction to this device will yield an infinite system with spatially periodic anchorage.



**Figure 2** Spatially Periodic Anchorage Schematic

### Topological Defects

Another characteristic of NLCs is that they often present topological defects, commonly known as disclinations, which relate to the head fields mentioned above. When there are abrupt changes of the directors or there is a very noticeable discontinuity, then we can say that there are disclinations.

There are two important types of disclinations in an NLC:  $D = 1/2$  intensity disclination and  $S = -1/2$  disclination to determine the intensity of a disclination in a CLN surrounds the defect region by plotting a circumference and Then it runs in the clockwise direction.

Analyzing how a vector tangent to the directing field rotates at each point in the path. In this way we can know how many turns the vector rotated (which indicates the magnitude of the disclination) and whether it did in the positive or negative direction (ie clockwise or counterclockwise).

### System to Simulate

The systems we simulate are thought of as working NLC in the experimental field, where a liquid crystal Pentil-cyano-biphenyl (5CB) is confined between two parallel plates separated by a distance of the order of microns, which are covered by a Layer on the inside very thin, ie a thin film of gold that can hold fixed the alternating anchorage between planar and perpendicular on the inner surfaces of both plates.

In the diagram of figure 3 we can observe the cell that we will use for our simulations: the vertical vectors in the first half represent the anchorage perpendicular to the plates and the horizontal vectors of the second half represent the planar anchorage, note that the anchorage is located in the horizontal direction (x-axis) and the plates that confine the liquid crystal are located in the vertical direction (normal to the z-axis). The angle  $\theta$  that determines the orientation of the planar anchor is measured with respect to the x-axis.

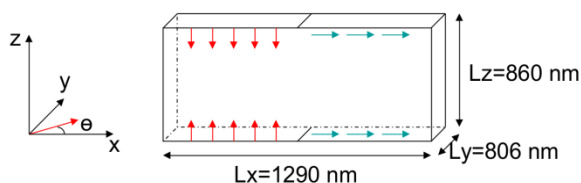


Figure 3 Simulation Cell

### Model

In order to predict the final orientation fields given certain initial conditions and to observe if they presented topological defects, we used a relaxation model that is a particular case of the Beris-Edwards model, which allows us to describe how the field of the order parameter evolves as it passes the time, by means of the alignment tensor  $Q$ :

$$\frac{\partial Q}{\partial t} = -\frac{1}{\gamma} \left[ \frac{\delta F}{\delta Q} \right] \quad (2)$$

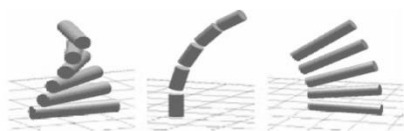
In the above equation, the alignment tensor  $Q$  is related to the directing field  $n$  as follows  $Q = S (nn - I / 3)$ , where  $S$  is the order parameter,  $I$  is the identity tensor,  $\delta$  denotes the functional derivative,  $F$  is the free energy functional and  $\gamma$  is a constant related to the coefficient of rotational diffusivity.

The free energy consists of two parts; the free energy of Landau de Gennes and elastic energy.

$$F[Q(r)] = \int A \text{tr}Q^2 + B \text{tr}Q^3 + C \text{tr}Q^4 + L(\partial_k Q_{ij})^2 dr \quad (3)$$

The coefficients  $A$ ,  $B$  and  $C$  are functions of temperature and  $L$  is the elastic constant that is related to the three types of distortion Aperture, Twist and Bend (Splay, Twist and Bend).

In this model equilibrium properties are described by the free energy of Landau de Gennes, in the following figure 4 we can observe the three types of distortions that appear in the liquid crystals, these are Torsion, Fold and Opening from left to right respectively



**Figure 4** Tipos de distorsiones

### Stationary solutions

In this project we are interested in the long-term stationary solutions in the relaxation model. To ensure that the simulations reached equilibrium, we took simulation times  $t$  much larger than the relaxation time  $\tau$  of the CL, which in the case of 5CB implies that  $t = 50 \text{ s} \gg \tau = 0.01 \text{ s}$ .

An additional complication is that random initial conditions were analyzed in the project, so that multiple realizations of these systems had to be performed.

By performing multiple simulations for the random cases we can rely more or make sure that the results were obtained with a high degree of precision compared to the current experimental techniques.

### Numerical Method

The algorithm used to solve the differential equations that were presented in the development of this research was that of Euler and the derivatives were evaluated with the numerical method of finite differences, on domains with a rectangular prism shape.

Solutions were calculated on periodic systems, to study the effect of finite size on the orientation structure obtained finally.

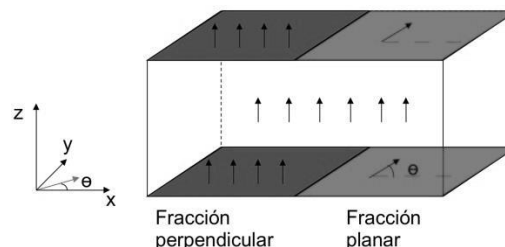
### Control Variables for Simulations

In general, the following cases were analyzed for the liquid crystal:

- Uniform Initial Configuration (homogeneous and homeotropic),
- Random Initial Setup

In each case the perpendicular fraction was modified in the x-direction, as well as the angle of the planar orientation with respect to the x-axis. That is, the main variables were the following illustrated in the diagram of figure 5.

- perpendicular fraction of the anchor in the x-direction (frac-perp)
- angle of the director  $n$  with respect to the x-axis (angle)
- initial direction of the directors between the plates (homeotropic, homogeneous and random)



**Figure 5** Diagrama de las variables de control

### Program code

For the development of this research we rely on the articles "Multiscale Simulations of Liquid Crystals" and "Monte Carlo simulations and dynamic field theory for suspended particles in liquid crystalline systems," focused on the Beris-Edwards liquid crystal relaxation model. These articles exploit computational techniques to simulate the evolution of a liquid crystal confined by a surface.

CRUZ-DIOSDADO, Leonardo David, HERNANDEZ-LOPEZ, Eymard, MATIAS-GUTIERRES, Sergio and LOPEZ-CASTRO, Roberto. Orientation of nematic liquid crystals with spatially periodic anchoring. ECORFAN Journal-Bolivia 2016.

Based on the aforementioned articles, changes were made to the programs developed by their authors: mainly a fixTensorAtPlates subroutine was modified to establish the periodic and alternating anchor, adding the new parameters (control variables, perpendicular fraction, angle of planar anchor and initial configuration of the liquid crystal) necessary to fulfill our objectives.

In order to make these changes to the basic programs, the knowledge of the Fortran 77 programming language had to be deepened. In the subroutine that establishes the parameters of the simulation from an input data file, the perpendicular limit that delimits the planar and perpendicular anchorage is added, as well as the angle of the planar orientation with respect to the x-axis. Variables were also introduced to represent the initial configuration of the liquid crystal.

We implemented a subroutine that fixes the initial condition of the liquid crystal inside the cell that is, start with the liquid crystal with a homeotropic, planar, and random configuration to study its behavior.

The execution of the program displays a table of numbers that represent the free energy of Landau, the elastic energy and the total energy with respect to the time, being difficult its interpretation, then with the help of software "Paraview" we were able to visualize both the parameter of order and the Directors and thus to make a more complete analysis regarding the degree of ordering as possible distortions in the liquid crystal.

## Results

### Simulated Cases

Basically, the following cases were analyzed for the liquid crystal: homogeneous homeotropic, planar and random initial configuration.

For each type of simulation, the control variables were changed: the perpendicular fraction was set at 25, 50 and 75 percent of the length of the cell in the x direction, while with respect to the angle of the planar orientation were used 30, 60 and 90 degrees with respect to the x-axis.

The size of the sides of the fundamental cell of said periodic arrangement was  $L_x = 1290$  nm,  $L_y = 20$  nm and  $L_z = 806$  nm.

### Liquid crystal initially homeotropic

As one of the objectives is to investigate the orientation of liquid crystals in devices that can be used in photonics, it is convenient to study the effect of varying the size of the cell to reach dimensions comparable to the wavelength of visible light.

We begin by studying the effect of varying the perpendicular anchorage fraction (fracperp) and the planar anchorage angle  $q$  when the initial condition in the cell is homeotropic.

In the case of the initial homeotropic configuration, it was observed that the initial orientation of the liquid crystal is preserved and that the perpendicular anchorage portion and the orientation of the planar anchorage are not relevant.

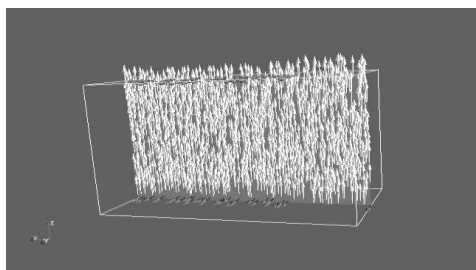


Figure 6 frac-perp=0.25, angle=60°

### Pulmonary fluid crystal

In the second system studied, the initial configuration was planar at an angle of zero degrees with respect to the x-axis, with a planar anchor at 60 degrees. The following figures illustrate the results for anchoring angle of 60 and 90 degrees.

A reorientation of the liquid crystal was observed in the same direction as the planar anchorage, regardless of the magnitude of the perpendicular fraction.

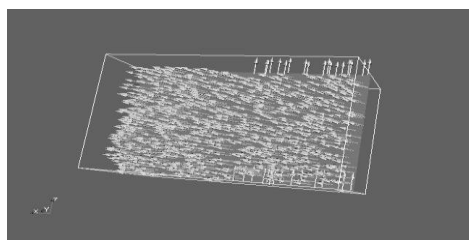


Figure 7 frac-perp=0.50, angle=60°

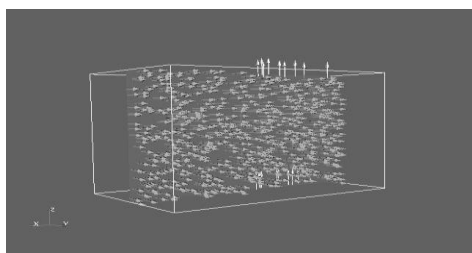


Figure 8 frac-perp=0.50, angle=90°

### Random liquid crystal

Finally, for the case where the initial configuration is random, the liquid crystal is reoriented according to the majority anchorage, be it planar or perpendicular. The following figure 9 shows this behavior:

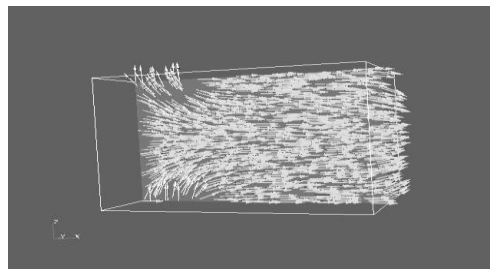


Figure 9 frac-perp=0.25, angle=0°

Finally, when we have an initially random configuration and a non-zero planar anchorage angle, we observe a reorientation of the liquid crystal in the direction of the majority anchorage.

Simultaneously we observe that the director deflects out of the x-plane and, noting that the director aligns partially with the z-axis. Figure 10 shows this effect (note the right end of the cell and how the directors do not point horizontally).

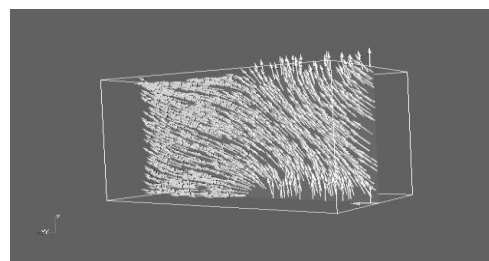


Figure 10 frac-perp=0.50, angle=30°

## Conclusions

From the simulations made, we are already prepared to be able to predict the final configuration that will be presented when arriving at the equilibrium for different initial configurations given.

The results can be reduced to three cases, according to the initial state of the liquid crystal between the plates: planar, homeotropic or random.

The final state depends on the initial state of the liquid crystal.

- If it starts with a homogeneous perpendicular configuration, no change is presented: that is, the initial configuration of the system is preserved, neither the perpendicular fraction of the anchor nor the planar part is oriented at a certain angle.
- If initially we have a planarly oriented medium, then the final orientation of the directing field ends aligned with the orientation of the planar anchorage and the perpendicular fraction is not relevant.
- Finally, if the initial configuration of the liquid crystal is random, the equilibrium is reached with a final configuration aligned in the direction of the majority anchorage. In addition, if the orientation of the planar anchorage is different from zero then a partial alignment with the vertical axis  $z$  is also present.

Another important aspect of the final configurations is that we could notice the presence of distortions in the double-aperture liquid crystal.

Finally it is very important to mention that through the simulations made it is possible to know the final orientation that the liquid crystals will take when reaching equilibrium, which is of great importance for the development of biomolecule detectors

## Prospects

The consequence of applying electric fields allowing to align the CL is very interesting. In the case of a parallel dipole, if the conductor adjusts to the applied field, then the electric field in the material is reduced by polarization effects and it turns out that the total energy of the system is also reduced. This is why it is intended in the near future to apply electromagnetic fields to the CLN system and determine what effects are observed in the presence of static electric and magnetic fields for different intensities.

Another important point is that, although this research does not take into account the effects of hydrodynamics of liquid crystals, this work can be used to make comparisons to those who work in the hydrodynamics of liquid crystals, since when comparing the results Obtained with and without hydrodynamic effects, a more complete analysis of the latter can be obtained, based on this work.

## References

- Jones R.A.L., *Soft Condensed Matter*, Oxford University Press, Oxford, 104-116 (2002).
- Lee et al. *Science* 291, 2576 (2001)
- O. Guzmán, N.L. Abbott and J.J. de Pablo, "Quenched disorder in a liquid-crystal biosensor: Adsorbed nanoparticles at confining walls", *Journal of Chemical Physics* 122, 184711 (2005).



O. Guzmán, Sylvain Grollau, E. B. Kim and J.J. de Pablo, "Multiscale simulation of liquid crystals", in *Computer Simulations of Liquid Crystals and Polymers* 221-247 Kluwer, Dordrecht (2005).

O. Guzmán and David Cruz, Programming code and simulations in fortran 77, 2008.

S. Grollau, E.B. Kim, O. Guzmán, N.L. Abbott and J.J. de Pablo, "Monte Carlo simulations and dynamic field theory for suspended particles in liquid crystalline systems", *Journal of Chemical Physics*, 119-4 (2003).

## **Rehabilitation of manufacturing equipment**

CASTILLO-ORTIZ, Jorge Iram \*†, ORTIZ-SIMÓN, José Luis and CRUZ-HERNÁNDEZ, Nicolás

*Instituto Tecnológico de Nuevo Laredo*

Received July 10, 2016; Accepted November 4, 2016

---

### **Abstract**

With the advice of some teachers Institute of Technology engineers Nuevo Laredo was achieved rehabilitate and operate an arm and a conveyor belt electro- pneumatic. Both machines were broken and does not work. The aim of this work was to restore an electron - pneumatic arm and a conveyor belt of a production line and have more teaching tool for student use. How these machines mentioned above were carried back to the operation described.

### **Technology, PLC, Solenoid**

---

**Citation:** CASTILLO-ORTIZ, Jorge Iram, ORTIZ-SIMÓN, José Luis and CRUZ-HERNÁNDEZ, Nicolás. Rehabilitation of manufacturing equipment. ECORFAN Journal-Bolivia 2016, 3-5: 16-18

---

---

\*Correspondence to Autohor: (iram\_castillo@live.com)

† Researcher contributing first author.

## Introduction

At present, technology is in constant progress and growth in greater proportion compared to past decades. Car models, electronic gadgets such as cell phones, home appliances, all show updates with improvements in both software and hardware or both. Therein lies the importance of also having school equipment (with which students can practice) in a constant update.

This document explains how an electro-pneumatic arm "Amatrol Flexible Manufacturing 2- 94 - FMS2" and a conveyor belt of the same brand were updated. In addition to the PLCs with which they were controlled (Allen Bradley obsolete), they were updated by Siemens of new generation.

## Materials and methods

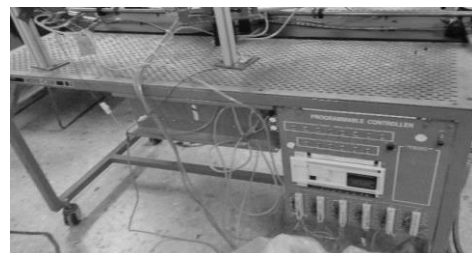
We were given (to the students who would perform this work) from our advisors, the electro-pneumatic arm and the conveyor belt under the conditions that can be seen in figures 1, 2 and 3. It was started making operational reviews in The conveyor belt. It was proved that the operation of the elements (solenoid valves, pistons, hoses, switches, wiring).



**Figure 1** Conveyor belt

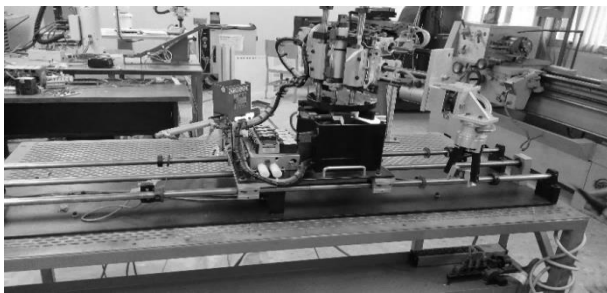
A compressor was placed and checked that there were no leaks in the hoses. The continuity of the switches was checked with a multimeter. After the functional tests were carried out, it was verified that the electrovalves were operated manually. The compressor was connected to the hoses and each electrovalve was individually checked. In solenoid valves that failed, they were opened and cleaned inside, they were rearranged their packaging. Of a total of 8 solenoid valves, one failed and was replaced. It was checked that there were no deterioration and / or damage in the conveyor chain. Wiring of valves and switches was separated and labeled for better organization.

For the pneumatic arm, it started in the same way as with the conveyor belt, checking and correcting faults. The electro-valves this time had damages that we only managed to make them work momentarily, therefore, our adviser opted to replace all the electro-valves. The wiring of each switch and valves was identified, so that connections to the new PLC could be made easier and the margin of error reduced.



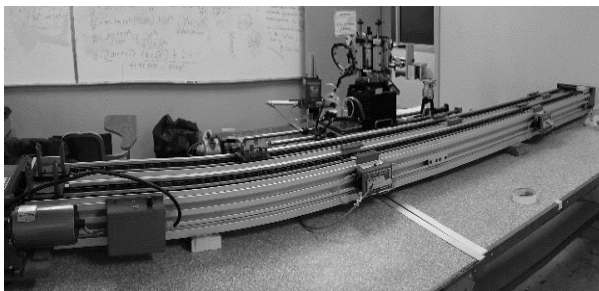
**Figure 2** Obsolete PLC's

Once the machines were already checked, the old PLCs were dismantled and the new ones were installed. The rest of the work was to make the connections between the 24V power supply with which the current, the electro-valves and the switches were to be supplied. Push buttons were also mounted to operate as a start and stop.



**Figure 3** Electro-pneumatic arm

A program was loaded onto the electro-pneumatic arm to verify that it was working completely. The results were favorable, the arm and the conveyor belt functioned in their entirety. Figure 4 shows the final result.



**Figure 4** Equipment rehabilitated

## Discussion

The greatest benefit obtained from a rehabilitation of this manufacturing equipment is that it will be very useful for the didactic use, being of support for both professors and students.

However, do not forget that the equipment is not new. Periodic maintenance is required to verify the condition of both the electro-pneumatic arm and the conveyor belt. Check the good functioning and that its components are in optimal conditions to reduce the probabilities of a future failure.

## References

Brühwiler, E. (2012, August). Rehabilitation and strengthening of concrete structures using ultra-high performance fibre reinforced concrete. In *Concrete Repair, Rehabilitation and Retrofitting III: 3rd International Conference on Concrete Repair, Rehabilitation and Retrofitting, ICCRRR-3, 3-5 September 2012, Cape Town, South Africa* (p. 30). CRC Press.

Walling, J. B. (1982). U.S. Patent No. 4,336,415. Washington, DC: U.S. Patent and Trademark Office.

Roy, S., & Irvin, R. (1983). *Sports medicine: prevention, evaluation, management, and rehabilitation*. Prentice Hall.

## Structural characterization of CdS doped with Pb<sup>2+</sup>

DÍAZ-REYES, J\*†', SÁNCHEZ-RAMÍREZ, J.F', FLORES-MENA, J.E"and MORÍN-CASTILLO, M.M "

*'Center for Research in Applied Biotechnology, Instituto Politécnico Nacional. Ex-Hacienda de San Juan Molino, Km. 1.5. Tepetitla, Tlaxcala. 90700. México*

*"Faculty of Sciences of the Electronics, Benemérita Universidad Autónoma de Puebla. Av. San Claudio y 18 Sur. Ciudad Universitaria. Puebla, Puebla. 72570. México*

Received August 14, 2016; Accepted November 1 2016

### Abstract

CdS nanocrystals doped with Pb<sup>2+</sup> are synthesised using a chemical bath deposition (CBD) growth technique under optimum conditions lead acetate at the reservoir temperature of 20±2°C. The Pb<sup>2+</sup> molar concentration was of 0.0≤x≤0.19.67 that was determined by EDS. The X-ray diffraction results show that the films are of PbS-CdS composites with individual CdS and PbS planes. The XRD analysis and Raman scattering reveal that CdS-deposited films showed zinc blende (ZB) crystalline phase. The mean grain size of the CdS films was ranged from 1.21-6.67 nm that was determined by Debye-Scherrer equation from ZB (111) direction and confirmed by high-resolution transmission electron microscopy (HRTEM). Raman scattering shows that the lattice dynamics is characteristic of bimodal behaviour and the multipeaks adjust of the first optical longitudinal mode for the Pb<sup>2+</sup>-doped CdS denotes the Raman shift of the characteristic peak in the range of 305-298 cm<sup>-1</sup> of the CdS crystals, which is associated with the lead ions incorporation.

### CBD, Semiconductor compounds II-VI, Raman spectroscopy, XRD

**Citation:** DÍAZ-REYES, J, SÁNCHEZ-RAMÍREZ, J.F, FLORES-MENA, J.E, Morín-Castillo, M.M. Structural characterization of CdS doped with Pb<sup>2+</sup>. ECORFAN Journal-Ecuador 2016, 3-5: 19-28

\* Correspondence to Author (email: joel\_diaz\_reyes@hotmail.com)

† Researcher contributing first author.

## Introduction

The development of third-generation solar cells overcoming the Shockley–Queisser efficiency limit for a single absorber, 31%, is one of the most fascinating challenges in the energy research field. In this aspect, semiconductor quantum dots (QDs) have shown extremely attractive properties for the development of solar cells overcoming the current limitations. The demonstration of an efficient multiple exciton generation (MEG) process in colloidal QDs, despite certain controversy, has aroused a huge interest in the use of these materials in photovoltaic devices.

This interest has been reinforced with the recent reports of absorbed photon-to-current efficiency (APCE) close to 200% and incident photon-to-current efficiency (IPCE) as high as 114%. In the former case PbS QDs have been employed in a sensitized solar cell configuration. An attempt was made to modify the band gap of CdS (~2.4 eV) by preparing a mixed lattice with a low-band-gap material, PbS (0.3 eV), giving a new set of materials, Cd<sub>1-x</sub>Pb<sub>x</sub>S.

Band gaps, as low as ~1.9 eV, were achieved with increasing x. It is a semiconductor with multiple applications in the technology field for its unique properties of detection, such as infrared detectors, photoresists solar cells for their ecological aspect and the effect of multiple exciton generation was recently discovered in PbS nanostructures, which is promising for such applications, for use in electronic applications thin films transistors (TFTs). Photosensitivity of detectors can be improved by adjusting the gate voltage and in the manufacture of laser diodes by its corresponding emission spectral range 2.7-4.2 μm [1].

In this work reports the growth and characterization of CdS: Pb<sup>2+</sup> nanofilms obtained by chemical bath deposition on glass substrate at low temperature. The effects of the chemical composition on structural properties of the CdS: Pb<sup>2+</sup> alloy were studied by X-ray diffraction, HRTEM, EDS, Raman scattering.

## Experimental details

The chemical bath is a technique to deposit and grow films on a solid substrate from a reaction that occurs in solution. It starts from an aqueous solution of salts of the elements of the compound to be obtained. It is required that the compound to deposit is relatively insoluble and chemically stable in the solution to give a simple precipitation in an ionic reaction [2].

For the synthesis of CdS: Pb<sup>2+</sup>, the metal ion source is lead acetate, hydroxyl ions source is sodium hydroxide, and the sulphur source is Thiourea ions and complexing agent, ammonium nitrate. All chemical reagents were from Sigma-Aldrich unless cadmium sulphate was Merck Millipore. The feasibility of this technique for its environment is: deposit short time, it does not require high temperatures, there is no emission of toxic gases into the atmosphere and the preparation of the solutions is carried out micro scale.

For carrying out the intentional doping by lead of the deposited layers is added small lead acetate volumes to the growth solution in the range of 0 to 30 ml to obtain different lead concentrations in the nanostructures, which are presented in Table 1. The CdS:Pb<sup>2+</sup> nanofilms chemical stoichiometry and surface morphology were obtained by SEM-EDS, which were carried out in a System LEO 438VP, with W.D. of 26 mm using a pressure of 20 Pa.

The crystalline phase and structure of the films were determined with a Bruker D8 Discover diffractometer using the copper  $K\alpha$  radiation ( $\lambda=1.5406 \text{ \AA}$ ) at 40 kV and 40 mA with parallel beam geometry. HRTEM studies were carried out in a JEOL JEM200 of 80-200 KV, the obtained image is recorded with a CCD camera in real time. The Gatan Digital Micrograph software was used for the analysis of HRTEM images. Raman scattering experiments were performed at room temperature using the 6328  $\text{\AA}$  line of a He-Ne laser at normal incidence for excitation. The light was focused to a diameter of 6  $\mu\text{m}$  at the sample using a 50x (numerical aperture 0.9) microscope objective. The nominal laser power used in these measurements was 20 mW.

## Results and discussion

The chemical composition of the  $\text{CdS:Pb}^{2+}$  films was estimated by EDS measurements, which besides allow to know the presence of some residual impurities. The EDS results indicate that besides the samples contain a significant amount of silicon, potassium, calcium, sodium and oxygen, and other residual impurities. Thus, the most of residual impurities detected in the layers come from of the substrate, which is corning glass.

The results of such measurements are shown in Table 1, in which is included the atomic and mass percentages. From these results is observed that sample M1, CdS, is not a stoichiometric compound and that starting from it a higher thiourea concentration in the solution gives a higher presence of cadmium and lead in the material and an absence of sulphur. Continuing with the consideration that each unit cell of CdS contains two cadmium atoms and two sulphur atoms, the atomic weight of the ideal unit cell is  $\sim 288.95$  corresponding to 22.19% sulphur atoms and 77.81% cadmium atoms.

Then, when a stoichiometric deviation of ideal unit cell occurs, it could establish a correspondence between vacancies or interstices of some of the compound elements (VS, VCd, Cdi, Si). In case of M1, it has excess of Cd and absence of sulphur, which is indicative that cadmium is interstitial and there are vacancies of sulphur.

The average errors with which were calculated percentage masses of different elements were for cadmium 1.25%, sulphur 0.35% and for lead 0.25%. As can see in Table 1, these errors do not significantly alter the above findings. Table 1 shows that the samples contain a lower S concentration, indicating that have a high concentration of sulphur vacancies. It can induce that there is a high concentration of cadmium and lead interstices. Therefore, the samples studied; there is excess elements II and IV and lack element VI.

Sample	$\text{Pb}(\text{C}_2\text{H}_5\text{O}_2)_2$ added volume (ml)	Cd mass weight (%)	Cd molar fraction (%)	S mass fraction (%)	S molar fraction (%)	Pb mass fraction (%)	Pb molar fraction (%)
M1	00	82.01	56.53	17.99	43.47	0.00	0.00
M2	05	74.06	52.33	18.26	44.21	7.68	3.45
M3	10	73.03	51.69	15.79	42.74	11.18	5.58
M4	15	61.19	48.29	12.71	38.10	26.10	13.61
M5	20	58.68	47.12	11.38	38.14	29.94	14.70
M6	25	56.90	45.83	11.27	38.46	31.83	18.72
M7	30	56.47	41.16	11.23	39.17	32.81	19.67

**Table 1** Summary of the  $\text{CdS:Pb}^{2+}$  samples grown and studied in this work. The Pb, Cd and S concentrations in deposited samples were estimated by EDS

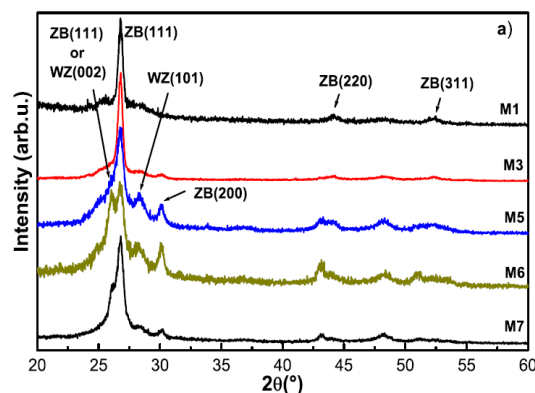
Figure 1a shows XRD patterns of  $\text{CdS:Pb}^{2+}$  nanofilms with different lead concentrations deposited at a temperature of  $20\pm 2^\circ\text{C}$ . It is observed from XRD patterns that  $\text{CdS:Pb}^{2+}$  films deposited are in polycrystalline nature. It can be seen that each peak corresponds fairly well with data of  $\text{CdS:Pb}^{2+}$  marked in the software DICVOL04 data.

The obtained structural parameters with the software DICVOL04 data are in good agreement with the published ones. From this close agreement, it is confirmed that as deposited CdS:Pb<sup>2+</sup> nanofilms for all the thiourea concentrations belong to the cubic crystal system. The X-ray patterns of deposited CdS:Pb<sup>2+</sup> thin films are described in the Fm-3m(225) and whose lattice parameters were calculated using the software DICVOL04, obtaining the following lattice parameters values:  $a = 5.73 \text{ \AA}$ , which are in agreement with the reported values [3]. CdS exists in two crystalline modifications: the wurtzite (WZ) [4] and zinc blende (ZB) phase.

As can be seen, the obtained diffraction pattern for sample M1 shows a predominant peak at  $2\theta = 26.81^\circ$ , which can be assigned to (111) plane of ZB CdS phase. Moreover, the intensity weak of peak at  $2\theta = 28.27^\circ$  is due to diffraction from the (101) plane WZ phase whereas at  $2\theta = 26.44^\circ$  position can be co-occupied by the (111) plane of ZB phase as well as the (002) plane WZ. However, the maximums peak intensity for both crystalline phases are different, ZB maximizes at  $2\theta = 26.81^\circ$  corresponding to the (111) plane, whereas WZ phase has its maximum intensity peak at  $2\theta = 28.20^\circ$  corresponding to (101) plane [5].

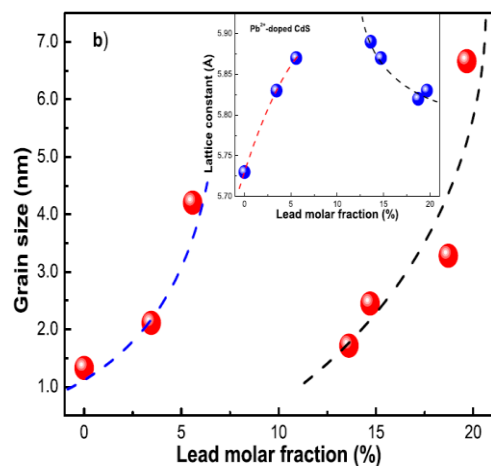
Formation of the WZ phase is likely, at least to large extent, because the characteristic diffraction peak from the (002) planes of the structure was completely absent when the CdS film was deposited. The shift in the diffraction angles are due to the incorporation of Pb<sup>2+</sup> at the sub-lattices sites of Cd<sup>2+</sup>. It has been reported in the literature that the probability that CdS dissolves in the PbS lattice at room temperature is very low [6]. In this case of extremely small particles, where the contribution of surface free energy is very important, some deviations cannot be excluded.

From XRD patterns can be assured that the Pb<sup>2+</sup> forms PbS according to the peak observed at  $2\theta \sim 30.01^\circ$  in M5 and M6 samples. Besides, it is observed a widening at the peak of the preferential (111) direction, which could be caused by undergoing stress, size of small crystalline domain or fluctuations in concentration. The first case does not happen since the used substrate is amorphous and it does not produce a mismatch in the material lattice parameters. The variation in the size of the average crystalline domain is the cause of this widening that can be due to the small size of the crystals



**Figure 1** XRD diffraction patterns for CdS and CdS:Pb films. M1 diffractograms displays peaks at:  $2\theta = 26.81^\circ$ ,  $44.16^\circ$  and  $52.44^\circ$ , which are related to the (111), (220) and (311) reflection planes for the CdS. ZB phase





**Figure 2** Dependence of the grain size of the average crystalline domain based on the increase of lead molar fraction for the CdS:Pb<sup>2+</sup> system. The inset shows lattice constant as function of Pb molar fraction

And by presence of strains that possess multiple facet diffraction peaks, which is the result of multidirectional growth of the synthesized nanocrystals. In fact to apply the Debye-Scherrer equation [7], one finds that the crystalline domain increases. The mean grain size was calculated from cubic (111) reflection of CdS:Pb<sup>2+</sup> for the all the studied samples. It is worth-noting the values of electronegativity for Pb (2.33) and Cd (1.69), which are favourable to form a solid solution [8].

These results show that the grain size increases as the thiourea concentration is increased in the growth solution as can be observed in Table 1 and Fig. 1a. Fig. 1b shows the variation of the size of the average crystalline domain with the lead incorporation obtained by the Debye-Scherer equation through the measurement of the width at half-maximum (FWHM) of the more intense peak that is (111) direction of deposited layers, which is sited about 26.81°. The intensity of this peak depends lightly of the lead molar fraction in the nanofilms.

The dash lines are some figures-of-merit for following the behaviour of experimental points, as is observed there are regions, the first one corresponds at low lead concentrations, M1, M2 and M3 samples, and second one to high lead concentrations, where clearly is observed the Pb<sup>+2</sup> effect to replace Cd ions of the CdS:Pb<sup>2+</sup> lattice. Similar behaviour is observed for the lattice constant, as shown in the inset of Fig. 1b. For the interplanar distance (ID) (111) for the ZB phase presented in Table 2, calculated from the 2θ peak position, versus lead molar fraction, increases lightly. This ID, in practice, coincides with (111) ID of the ZB phase. It can be seen that it increases as V [Pb<sup>+2</sup>] increases, suggesting the formation of a solid solution and then it goes up again, having a region of discontinuity, for higher V [Pb<sup>+2</sup>].

This is consistent with a single phase material at lowest V [Pb<sup>+2</sup>] and a two-phase material at higher V [Pb<sup>+2</sup>]. Moreover, the lattice constant increases with increasing V [Pb<sup>+2</sup>] in the film which is an effect of Pb<sup>2+</sup> substituting Cd<sup>2+</sup> in CdS. A possible explication to this experimental fact can be due to difference of the ionic radii of Cd<sup>2+</sup> (0.97 Å) and Pb<sup>2+</sup> (1.20 Å). The (111) ID of ZB phase in bulk are 3.367 Å.

These values are larger than the ID values found for the CdS-CdSPb films in this work. It is probable that values of ID in CdS:Pb<sup>2+</sup> nanofilms are owing to the existence of Cd<sup>2+</sup> vacancies.

For a relative low concentration of  $\text{Pb}^{2+}$  ion, this can be, in a large majority, be situated in: (a)  $\text{Cd}^{2+}$  vacancies sites which otherwise would be empty [9], (b) in  $\text{Cd}^{2+}$  sites provoking the appearing of  $\text{Cd}^{2+}$  interstitial, and (c) in interstitial positions. For higher V [ $\text{Pb}^{2+}$ ], the material behaves like a solid solution, the generation of  $\text{Cd}^{2+}$  vacancies, whose creation is needed to charge balance, start to be important in number and given the relative ionic radius of  $\text{S}^{2-}$ .

There is a tendency of the Full Width at Half Maximum (FWHM) of (111) peak [2] of the grown films probably due to all of the possible  $\text{Pb}^{2+}$  species present in  $\text{Cd}^{2+}$  sites and interstitials positions, and also to the existence of PbS, which distort the crystalline lattice and provoke structural disorder. The distortion produces a strong strain that affects the

Sample	$a_{\text{X-ray}}$ (Å)	$d_{(111)}$ (nm)	Grain size (X-ray) (nm)	Grain size (TEM) (nm)	Bandgap I (eV)	Bandgap II (eV)	Bandgap III (eV)
M1	5.73	0.28	2.12	5.11	2.49	1.67	0.98
M2	5.83	0.29	1.33	+-	2.45	1.97	2.09
M3	5.87	0.29	1.21	5.50	2.44	1.96	2.06
M4	5.89	0.31	1.72	---	2.49	1.99	2.01
M5	5.87	0.33	2.45	5.85	2.46	1.84	
M6	5.84	0.33	3.28	3.50	2.34	1.77	
M7	5.83	0.33	6.67	--	2.27	1.71	

**Table 2** The mean grain sizes of the nanofilms obtained by the Debye-Scherrer equation for the direction ZB (111), which show the dependence of the grain size of the average crystalline domain based on the increase of Pb molar fraction for the  $\text{CdS:Pb}^{2+}$  system. Besides, it presents the grain sizes obtained by TEM. Additionally, it is shown the interplanar distance

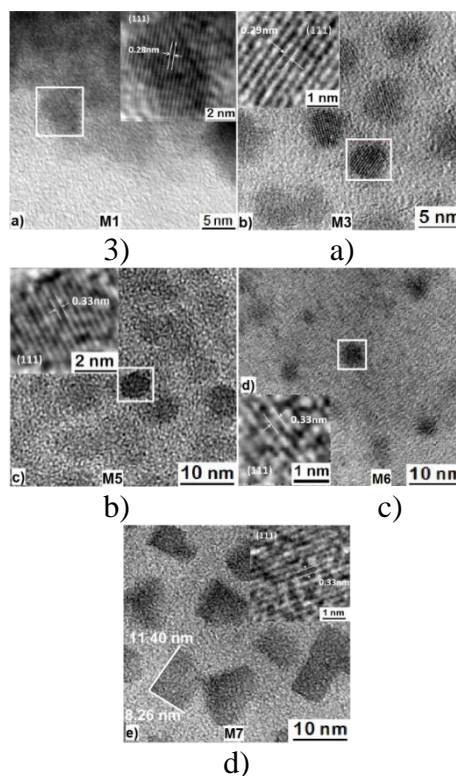
Interatomic distances; this similar fact has already been reported [10]. In this work, the strain and distortion of the lattice can be smaller. The appearing of  $\text{S}^{2-}$  ions into the material favours the relaxing of the lattice. Fig. 2 illustrates images obtained by high-resolution transmission electron microscopy for some typical samples, and the insets are the result of the processing of the HRTEM image using filters in Fourier space.

As is observed in figures there is two structure types, at low V [ $\text{Pb}^{2+}$ ] the crystal nanostructures are nearly spherical shape of the material with an average size of  $\sim 1.33$ - $6.67$  nm, and to the sample with higher V [ $\text{Pb}^{2+}$ ] contains nanostructures boxes shape, whose dimensions are approximately  $(11.30$ - $12.82)$  nm  $\times$   $(6.32$ - $8.72)$  nm, see Fig. 2d. This behaviour has been observed in other materials, that by changing the concentrations of the precursors or the experimental conditions the nanoparticles shape changes.

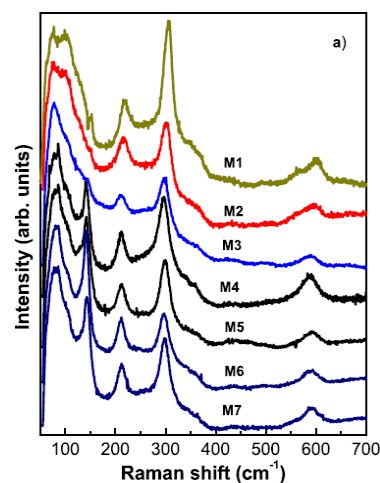
The most direct way of controlling the reaction kinetics, and thus particle shape, in these syntheses is by changing the concentration of the lead reducing agent. Increasing the amount of lead in the growth solution increases the rate of lead ion reduction, which should create a preference for the growth of more kinetically favourable (or less thermodynamically favourable) particle morphologies [11]. In addition in the insets can see clearly the distance interplanar of material, which corresponds to the direction of the cubic phase of the  $\text{CdS:Pb}^{2+}$  (111). As can be seen, the results obtained by HRTEM are in good agreement with the results calculated from XRD using the Debye-Scherrer equation.

The structural characterization of the synthesized CdS nanostructures was therefore carried out using Raman spectroscopy. Each of the phonon wavenumbers was extracted by fitting the Raman spectrum to a Lorentz line shape, and the first longitudinal optical (1LO) and second longitudinal optical (2LO) phonons and multiphonon processes can be clearly observed in Figure 3a, which correspond a zincblende (ZB) crystalline phase. For a better analysis the Raman spectra will be divided into two frequency ranges.

The first region for frequencies below 200  $\text{cm}^{-1}$  and the second one to higher frequencies as are illustrated in Figs. 3b-c, in which Raman spectra of three typical samples, M1, M2 and M7, are displayed. In Fig. 3b illustrates the CdS:Pb<sup>2+</sup> Raman spectra in the range from 50 to 200  $\text{cm}^{-1}$  for the three typical samples, M1, M2 and M7, showing three vibrational bands, which depend strongly on the lead molar fraction. Besides, it is observed that these bands happened a blue shift as lead concentration is increased. Similar vibration modes were obtained by Raman theories and are in agreement with the results reported by de Wijs et al. [12]. They are the typical characteristic peaks of the zincblende phase at low frequencies that were obtained by deconvolution using Lorentzian curves for finding the peaks frequency that are associated to



**Figure 3** HRTEM micrographs of the CdS:Pb<sup>2+</sup> samples: a) M3, b) M5, c) M6 and d) M7



**Figure 4** a) Raman spectra of the CdS:Pb<sup>2+</sup> films added with different lead concentrations. Deconvolution of the spectra for two Raman shift ranges: (a) lower one and (b) higher one

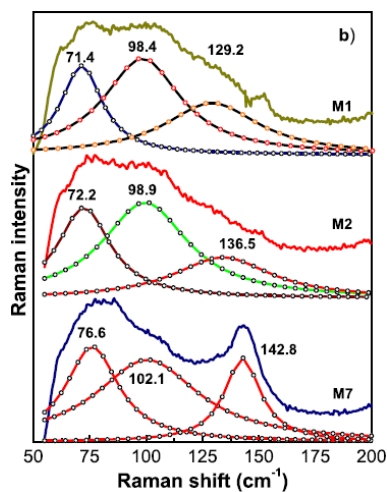


Figure a)

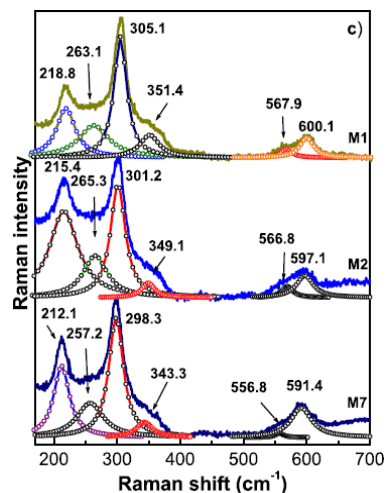


Figure b)

Lattice modes [13]. As is observed in Figs. 3, from M4-M7 Raman spectra the peak about 143 cm<sup>-1</sup> is well-resolved and can be associated to the combination of longitudinal and transverse acoustic phonon modes in PbS nanocrystals [14]. Then, the second frequency region will be discussed. The Raman peaks of M1 (nanoparticles) appear at 305.1 cm<sup>-1</sup>, attributed to the A<sub>1</sub>(LO) mode with a full width at half maximum (FWHM) of ca. 24.3 cm<sup>-1</sup> and its overtone at 600.2 cm<sup>-1</sup>. The Raman peaks of M2 (nanoparticles) appear at 301.2 cm<sup>-1</sup> with a FWHM of ca. 28.3 cm<sup>-1</sup> and its overtone at 597.1 cm<sup>-1</sup>.

The Raman peaks of M7 (nanoparticles) appear at 298.3 cm<sup>-1</sup> with a FWHM of ca. 28.1 cm<sup>-1</sup> and its overtone at 591.4 cm<sup>-1</sup> [15]. As is observed of these results Raman peaks are redshifted as lead concentration is increased in the nanofilms and the Raman spectra exhibit relatively sharp crystal-like peaks. The light increase of the FWHM from M1 to M2 and M7 can be attributed to a slight deterioration of the crystallinity of the CdS nanocrystals due to the incorporation of lead to Cd sub-lattice. It has been reported that defect-free crystalline CdS films have a FWHM of 8 cm<sup>-1</sup> [16].

Therefore, grown samples have a high density of structural defects, as had been deduced from the results of the chemical composition. We all know that in a crystalline semiconductor or insulator the observed Raman shifts usually correspond to the LOs, whereas other modes such as the transverse optical and surface phonon modes are not observable because of symmetry restrictions and their low intensities [17]. Another observation is that the peak profile of the nanoparticles is almost symmetric for the three samples.

It is also observed that the intensity of the Raman line LO of sample M2 is lower than that of M1, which is attributed to the quantity of the sample detected by Raman, see Fig. 4a. It is known that the intensity of a Raman line is proportional to the number of scattering centres because of the fact that Raman scattering is an incoherent process [18], in this case, as can be seen in Fig. 4b, the lattice vibrational frequencies are dominant and shielding to the longitudinal optical vibrations, as the V[Pb<sup>2+</sup>] increases.

In addition to the LO phonon and its replicas, and lattice vibrations, for sample M1, several peaks are resolved as 263.1, 351.4, and 567.9 cm<sup>-1</sup> suggesting that the samples have better crystalline quality [19].

The peaks at approximately, 263.1, 351.4 and 567.9  $\text{cm}^{-1}$  can be assigned to multiphonon scattering, which is consistent with other reports [20]. The feature at the high-energy shoulder, sited at 351.4  $\text{cm}^{-1}$ , is the subject of a recent study by Dzhagan et al. [21], who suggest that it results from the participation of acoustic phonons to the scattering process and the mode corresponding to the low-energy shoulder originates from surface optical phonon modes (SO) at 263.1  $\text{cm}^{-1}$  [22]. As is observed in Figs. 4b-c, the frequencies of the vibrational bands decrease as the lead molar fraction increases, this is consistent because of the ionic radius of lead is higher than cadmium.

## Conclusions

In this work presented the growth and characterization of  $\text{CdS:Pb}^{2+}$  nanofilms obtained by CBD technique by under our proposed reactant species and at  $20 \pm 2^\circ\text{C}$  as deposited temperature. The results of the studies of X-ray diffraction and Raman spectroscopy showed that grown  $\text{CdS:Pb}^{2+}$  nanofilms belong to the zincblende crystalline systems. The mean grain sizes of the nanocrystals are in the range of 1.21-6.67 nm, which were determined using the Debye-Scherrer equation for the ZB(111) direction and that were confirmed by HRTEM, although with this technique were obtained larger sizes.

This mean grain size indicates a high quantum confinement. Raman scattering showed that the lattice dynamics is characteristic of bimodal behaviour and the multipeaks adjust of the first optical longitudinal mode for the  $\text{CdS:Pb}$  denotes in all cases the Raman frequency of the characteristic peak is in the range of 305-298  $\text{cm}^{-1}$  of the  $\text{CdS}$  nanocrystals associated with the lead.

## References

- [1] Jeff Hecht, Understanding Lasers, 2nd ed., IEEE Press, New York NY(USA), 1994.
- [2] J.I. Contreras-Rascón, J. Díaz-Reyes, J. E. Flores-Mena, M. Galván-Arellano, L. A. Juárez-Morán, R. S. Castillo-Ojeda. *Curr. Appl. Phys.* 15 (2015) 1568
- [3] J. Singh. *Physics of Semiconductors and their heterostructures*. Ed. McGraw-Hill, 1993.
- [4] A. Abdolazadeh Ziabari, F. E. Ghodsi. *J. Lumin.* 141 (2013) 121.
- [5] G. Murugadoss. *Superlattice Microst.* 52 (2012) 1026.
- [6] M. Guglielmi, A. Martucci, J. Fick, G. Vitrant. *J. Sol-Gel Sci. Technol.* 11 (1998) 229.
- [7] J. A. Dean, Lange's. *Handbook of Chemistry*, 13th ed. (New York: McGraw-Hill. 1987).
- [8] R. Ortega-Borges, D. Lincot. *J. Electrochem. Soc.* 140 (1993) 3464.
- [9] M. Grus, A. Sikorska. *Physica B: Condensed Matter* 266 (1999) 139.
- [10] M. Esmaili, A. Habibi-Yangjeh. *Chin. J. Catal.* 32 (2011) 933.
- [11] M. R. Langille, M. L. Personick, J. Zhang, Ch. A. Mirkin. *J. Am. Chem. Soc.* 134 (2012) 14542.
- [12] G. A. de Wijs, R. A. de Groot. *Electrochim. Acta* 46 (2001) 1989.
- [13] A. Rougier, F. Portemer, A. Quédé, M. El Marssi. *Appl. Surf. Sci.* 153 (1999) 1.
- [14] G. D. Smith, S. Firth, R. J. H. Clark, M. Cardona. *J. Appl. Phys.* 92 (2002) 4375.

[15]E. J. Donahue, A. Roxburgh, M. Yurchenko. *Mater. Res. Bull.* 33 (1998) 323.

[16]M. Froment, M. Claude-Bernard, R. Cortes, B. Mokili, D. Lincot. *J. Electrochem. Soc.* 142 (1995) 2642.

[17]K. K. Nanda, S.N. Sarangi, S.N. Sahu, S.K. Deb, S.N. Behera. *Physica B: Condensed Matter* 262 (1999) 31.

[18]H. Brunner, H. Sussner. *Biochim. Biophys. Acta* 271 (1972) 16.

[19]V. Sivasubramanian, A.K. Arora, M. Premila, C.S. Sundar, V.S. Sastry. *Physica E: Low-dimensional Systems and Nanostructures* 31 (2006) 93.

[20]S. Kar, B. Satpati, P. V. Satyam, S. Chaudhuri. *J. Phys. Chem. B* 109 (2005) 19134.

[21]V. M. Dzhagan, I. Lokteva, M. Ya. Valakh, O. E. Raevska, J. Kolny-Olesiak, D. R. T. Zahn. *J. Appl. Phys.* 106 (2009) 084318.

[22]F. Comas, Nelson Studart, G.E. Marques. *Solid State Commun.* 130 (2004) 477.

## Instructions for authors

---

### [Title in Times New Roman and Bold No.14]

Last name -First name, (in uppercase) -1st † Last name -First name (in uppercase) -2nd Author's name

*Institutional mail No.10 Times New Roman and Italic*

(Report Submission Date: Month, Day, and Year); accepted (Insert date of Acceptance: Use Only ECORFAN)

---

### Abstract

Title

Objectives, methodology

Contribution

(150-200 words)

Keywords

Indicate (3-5) keywords in Times New Roman and Bold No.11

---

**Citation:** Last name -First name (in uppercase) -1st † Last name -First name (in uppercase) -2nd Author's name. Paper Title. Title of the Journal. 2016 1-1: 1-11 - [All in Times New Roman No.10]

---

---

† Researcher contributing as first author.

## Instructions for authors

---

© ECORFAN-Bolivia

[www.ecorfan.org/bolivia](http://www.ecorfan.org/bolivia)

### Introduction

Text in Times New Roman No.12, single space.

General explanation of the subject and explain why it is important.

What is your added value with respect to other techniques?

Clearly focus each of its features

Clearly explain the problem to be solved and the central hypothesis.

Explanation of sections Article.

### Development of headings and subheadings of the article with subsequent numbers

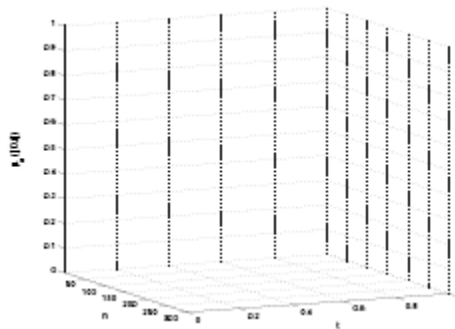
[Title No.12 in Times New Roman, single spaced and Bold]

Products in development No.12 Times New Roman, single spaced.

### Including graphs, figures and tables-Editable

In the article content any graphic, table and figure should be editable formats that can change size, type and number of letter, for the purposes of edition, these must be high quality, not pixelated and should be noticeable even reducing image scale.

[Indicating the title at the bottom with No.10 and Times New Roman Bold]



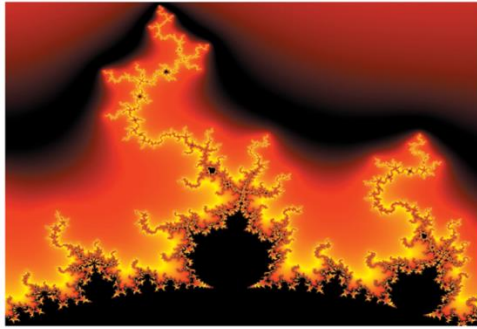
**Graphic 1** Title and Source (in italics).

Should not be images-everything must be editable.



# Instructions for authors

---



**Figure 1** Title and Source (in italics).

Should not be images-everything must be editable.


**Table 1** Title and Source (in italics).

Should not be images-everything must be editable.

Each article shall present separately in **3 folders**: a) Figures, b) Charts and c) Tables in .JPG format, indicating the number and sequential Bold Title.

**For the use of equations, noted as follows:**

$$Y_{ij} = \alpha + \sum_{h=1}^r \beta_h X_{hij} + u_j + e_{ij} \quad (1)$$

They must be editable and number aligned on the right side.

## Methodology

Develop give the meaning of the variables in linear writing and important is the comparison of the used criteria.

## Results

The results shall be by section of the article.

## Annexes

Tables and adequate sources thanks to indicate if they were funded by any institution, University or company.

# Instructions for authors

---

## Conclusions

Explain clearly the results and possibilities of improvement.

## References

Using APA system, should **Not** be numbered, either bulleted, however, if necessary, will be because reference number or referred to in any of the article.

## Data Sheet

Each article must submit your dates into a Word document (.docx):

Journal Name

Article title

Abstract

Keywords

Article sections, for example:

1. *Introduction*
2. *Description of the method*
3. *Analysis from the regression demand curve*
4. *Results*
5. *Thanks*
6. *Conclusions*
7. *References*

Author Name (s)

Email Correspondence to Author

References



Sucre-Bolivia \_\_\_\_\_, \_\_\_\_\_ 20 \_\_\_\_\_

**ECORFAN®**

**Originality Format**

I understand and agree that the results are final dictamination so authors must sign before starting the peer review process to claim originality of the next work.

---

Article

---

Signature

---

Name



ECORFAN®

Sucre-Bolivia \_\_, \_\_\_\_ 20 \_\_

### Authorization form

I understand and accept that the results of evaluation are inappealable. If my article is accepted for publication, I authorize ECORFAN to reproduce it in electronic data bases, reprints, anthologies or any other media in order to reach a wider audience.

---

Article

---

Signature

---

Name

# ECORFAN Journal-Bolivia

*"Implementation of improvement in a production line for the production of meat in canal and primary cuts"*

ANTONIO-ANTONIO, Alejandrina, MEZA-MORALES, Martha Isis, VAZQUEZ-FERNANDEZ, Jorge Alberto, RUIZ-PEREZ, Cinthia Daniela

*"Orientation of nematic liquid crystals with spatially periodic anchoring"*

CRUZ DIOSDADO, Leonardo David , HERNANDEZ-LOPEZ, Eymard, MATIAS GUTIERRE,S Sergio, LOPEZ-CASTRO, Roberto  
Tecnológico de Estudios Superiores del Oriente del Estado de México.

*"Rehabilitation of manufacturing equipment"*

CASTILLO-ORTIZ, Jorge Iram , ORTIZ-SIMÓN, José Luis, CRUZ-HERNÁNDEZ, Nicolás  
Instituto Tecnológico de Nuevo Laredo

*"Structural characterization of CdS doped with Pb<sup>2+</sup>"*

DÍAZ-REYES, J', SÁNCHEZ-RAMÍREZ, J.F', FLORES-MENA, J.E", MORÍN-CASTILLO, M.M"

' Instituto Politécnico Nacional

" Benemérita Universidad Autónoma de Puebla



[www.ecorfan.org](http://www.ecorfan.org)